High-resolution Controllable Prostatic Histology Synthesis using StyleGAN

Gagandeep B. Daroach[1], Josiah A. Yoder[1], Kenneth A. Iczkowski[2] and Peter S. LaViolette[2]
[1]*Electrical Engineering and Computer Science, Milwaukee School of Engineering, Milwaukee, WI 53202, U.S.A.*
[2]*Radiology and Biomedical Engineering, Medical College of Wisconsin, Wauwatosa, WI 53226, U.S.A.*

Keywords: Medical Imaging, Histology, Prostate, Prostate Cancer, Deep Learning, Machine Learning, Latent Space, GAN, StyleGAN, StyleGAN2, Generative Adversarial Networks, Gleason.

Abstract: For use of deep learning algorithms in clinical practice, detailed justification for diagnosis is necessary. Convolutional Neural Networks (CNNs) have been demonstrated to classify prostatic histology using the same diagnostic signals as pathologists. Using the StyleGAN series of networks, we demonstrate that recent advances in high-resolution image synthesis with Generative Adversarial Networks (GANs) can be applied to prostatic histology. The trained network can produce novel histology samples indistinguishable from real histology at 1024x1024 resolution and can learn disentangled representations of histologic semantics that separates at a variety of scales. Through blending of the latent representations, users have the ability to control the projection of histologic semantics onto a reconstructed image. When applied to the medical domain without modification, StyleGAN2 is able to achieve a Fréchet Inception Distance (FID) of 3.69 and perceptual path length (PPL) of 33.25.

1 INTRODUCTION

Prostatic cancer is one of the most common malignancies in men across the globe, ranking second after lung cancer (Rawla, 2019). Prostatic cancer is diagnosed with a biopsy and often treated with radical prostatectomy. Recent advances in the machine learning medical imaging domain introduce convolutional neural networks (CNNs) that can assist pathologists with diagnosing Gleason patterns indicative of patient prognosis from histology (Young et al., 2019; Li et al., 2019; Araújo et al., 2017) and generative adversarial networks (GANs) that are able to reconstruct novel medical images from a latent code or label (Kazeminia et al., 2018; Karras et al., 2020). Efforts to improve automated Gleason grading are ongoing (MICCAI, 2020). To best combine a pathologist's diagnostic skill with a neural network, both the network and pathologist need to be able to share explanations in support of their decisions with one another. As a result, there has been much work on interpreting how a deep neural network comes to the decision that it does (Du et al., 2019; Li et al., 2019).

Karras et al. demonstrate new techniques for increased interpretability of image reconstruction with the StyleGAN series of networks (ProgGAN, StyleGAN, and StyleGAN2) (Karras et al., 2018; Karras et al., 2019; Karras et al., 2020). In a review of interpretable models, Du et al. point out that many machine learning models sacrifice accuracy for interpretability (Du et al., 2019). In contrast, StyleGAN networks gain interpretability while improving the state of the art. The modern network architecture stabilizes reconstruction of high resolution (1024x1024) images (Karras et al., 2018) and layer normalization disentangles latent representations for enhanced user control of image semantics (Karras et al., 2019; Karras et al., 2020) in diverse non-medical domains. For example when reconstructing human face imagery, StyleGANs can control facial features including smile, hair color, and age (Karras et al., 2020; Karras et al., 2019; Karras et al., 2018). StyleGAN2 eliminated high resolution artifacts common in image reconstruction with an updated style control mechanism (Karras et al., 2020) while simplifying training complexity.

The Gleason grading system for prostatic adenocarcinoma originated in the 1960-70s and has been developed further by the International Society of Urologic Pathology in 2005 and 2014 (Chen and Zhou, 2016). Both pathologists and clinicians need

Daroach, G., Yoder, J., Iczkowski, K. and LaViolette, P.
High-resolution Controllable Prostatic Histology Synthesis using StyleGAN.
DOI: 10.5220/0010393901030112
In *Proceedings of the 14th International Joint Conference on Biomedical Engineering Systems and Technologies (BIOSTEC 2021) - Volume 2: BIOIMAGING*, pages 103-112
ISBN: 978-989-758-490-9

to fully understand the principles and practice of the Gleason grading system to effectively diagnose patients. Classification of Gleason grade is done solely based on visual morphologies in hematoxylin-eosin stained histology (Chen and Zhou, 2016). The principal motivation of this study is to investigate how StyleGAN captures these morphologies and relates histologic semantics in the input latent space. The GAN reconstruction network learns to relate visual morphologies during the unsupervised training period with feedback from a CNN analyzing the unlabeled histologic training data. The machine learning developed relations in these convolutional feature maps may provide new insights into Gleason grading patterns.

In this paper, our contributions are:

- We demonstrate GANs can produce novel prostatic histology at a high-resolution (1024^2) and accurately capture features of prostatic histology including stroma, benign tissue, atrophy, low-grade, and prostatic cancer. A pathologist was unable to distinguish between the real and generated images (Section 5.1)
- We demonstrate StyleGAN and StyleGAN2 embed histologic morphology to different generator deep layers, isolating high (gland, lumen shape), medium (epithelium and stroma texture), and low-level (coloration, nuclear density) pathological features for user control (Section 5.2)
- We propose a strategy for preparing whole slide images into a high resolution training dataset to maximize the performance of GAN image reconstruction. (Section 4.1)

2 RELATED WORK

There is uncertainty in the literature as to whether GANs improve interpretability over other deep networks. Some authors promote the use of GANs for interpretation (Chen et al., 2018; Skandarani et al., 2020) while others point out the work that remains (Kazeminia et al., 2018). Themes for improving interpretability include inverting images to the latent space (Chen et al., 2018; Karras et al., 2020), demonstrating separability of morphological labels in the latent space (Skandarani et al., 2020; Quiros et al., 2020), and combining the GAN with existing methods (Kazeminia et al., 2018; Skandarani et al., 2020). In this study, we find that StyleGAN separates histologic morphologies at different scales, correlates morphologies with latent values, and maps stoichastic information in the noise channel to determine the specific placement of the image features.

Some authors have explored variations of the original StyleGAN on medical images. Xu et al. use a modified GAN architecture inspired from StyleGAN components and MCGAN to draw non-small cell lung cancer (NSCLC) nodules onto chest CT imagery (Xu et al., 2019). Given a 128^2 portion of a chest CT and a patient's protein profile, the GAN realistically projects NSCLC nodules into the chest medical image. Quiros demonstrate accurate prostatic histology reconstruction at 224^2 and 448^2 resolution using PathologyGAN, inspired from the StyleGAN and BigGAN networks, to achieve a FID of 16.65 (Quiros et al., 2020). In this study, we use 1024^2 images as in the original StyleGAN networks and explore which histological features are captured at each layer.

Karras et al. explored training StyleGAN networks on limited data, including the breast histology dataset BRECAHAD, proposing an adaptive data augmentation technique for training algorithms on small datasets containing only hundreds of 1024^2 images rather than tens of thousands (Karras et al., 2020). In this study, we train on hundreds of thousands of high quality images, so small-training set techniques are not required.

3 BACKGROUND

Generative Adversarial Networks. The adversarial learning framework is a pivotal contribution to the data generation field, enabling synthesis networks capable of producing novel samples from high-dimensional data distributions (Goodfellow et al., 2014). An image GAN consists of an inverse CNN synthesis network (generator or G) and a traditional CNN classification network (discriminator or D).

Learning happens in three discrete stages. First D classifies a batch of random images from the input domain as real or fake, embedding real image semantics in its convolutional feature maps. Second G samples a batch of random latent codes and presents fake data to D. Third D grades the realism of the fake data, producing a loss gradient for G to update with the information in D's convolutional feature maps. Training concludes when D is unable to distinguish between samples from the training distribution and the synthetic distribution produced by G.

Progressive Growing. ProgGAN introduced the notion of progressive growing of image data to stabilize training of higher-resolution images (Karras et al., 2018). In StyleGAN the training images are

down-sampled to 4^2 resolution and doubled in spatial size after each epoch until the target 1024^2 resolution. Karras et al. hypothesize that lower-resolution data is more stable to learn because there are fewer modes, and as the learning progress the modes can be divided while maintaining the structure shared by the modes. In some sense, the course layers/features learned early in training provide scaffolding for the later layers to learn fine details.

Intermediary Latent Space. The input latent space Z is modeled as a vector of uncorrelated Gaussian noise. StyleGAN uses a multi-layer fully-connected network (the transformer) to map the input Z space onto an intermediary latent space W before feeding into the synthesis network. The W space has an advantage over the Z space in that it is not constrained to a multivariate single-modal Gaussian distribution. If the space of training images is not naturally represented by a Z hyper-sphere, the transformer can learn to map the hyper-sphere onto a more natural, disentangled latent space W.

For instance, if G is trained on images that have variations in H&E staining such that cribiform appears in dark purple stains and healthy stroma appears in light pink stains, there may exist a combination of cribiform in light pink and stroma in dark purple in the W space although not explicitly in the training data. In StyleGAN, the disentangled latent space can map onto image semantics at multiple scales of the synthesis network because the W space interacts with each convolutional upsampling layer twice.

4 METHODS

4.1 Prostatic Histology Data Preparation

Thirteen (13) patients with biopsy-confirmed prostatic cancer were included in this study. Following radical prostatectomy, samples were sectioned using patient-specific slicing jigs created from the presurgical magnetic resonance images (McGarry et al., 2019). Tissue sections were paraffin-embedded, whole-mounted, stained with hematoxylin-eosin (H&E), and then digitally scanned using a Huron microscope at 40X magnification or 0.20 µm per pixel. JPEG compression reduced the average ~120GB raw whole slide image (WSI) TIF files into ~15GB TIF images while retaining 90% of perceived image quality.

Each WSI was down-sampled by a factor of 2 to visualize both small cell features and large tissue features at 1024^2 image size. A vector processing pipeline approach (Martinez and Cupitt, 2005) was applied to incrementally process each WSI into 1024^2 PNG images without loading the complete WSI into computer memory. To remove white tiles and low-quality tiles from the edges of the slide scan, an HistomicsTK algorithm was used to count the number of nuclei in each tile (Gutman et al., 2017). Two datasets were created for evaluation of the models. To construct the *Simple* dataset, image tiles with 100 or more nuclei were extracted, resulting in 87k tiles. For the *Augmented* Dataset, first tiles with more than 20 nuclei were extracted, resulting in 100k tiles. Next each image was augmented with a horizontal flip and four 90 degree rotations yielding eight tiles per each input tile or 800k total images. In both datasets, each image was down-sampled into nine levels with spatial dimensions ranging from 4^2 to 1024^2 before feeding into the progressive growing training process (Karras et al., 2018).

4.2 StyleGAN Training

The StyleGAN (Karras et al., 2019) and StyleGAN2 (Karras et al., 2020) networks were each trained twice, once on the *Simple* dataset and once on the *Augmented* dataset. The networks from the official NVLabs GitHub repositories were configured with the default large network architecture *Config-F*. Each training run was done with eight NVIDIA V100's in a DGX-1 system. StyleGAN trained through 25 million real image impressions, and StyleGAN2 through 21 million.

5 RESULTS

5.1 Quantifying Generator Performance

The generator performance is measured using the Fréchet inception distance (FID) and perceptual path length (PPL). Rather than pixel-wise comparisons (as done by the L2 norm), the FID metric uses a pre-trained VGGnet CNN to compare visual similarity between real and synthetic images, mimicking human perception (Heusel et al., 2017). PPL is an auxiliary metric introduced in (Karras et al., 2020) that measures how well the disentangled latent space fits onto correlated features and grades overall semantic consistency within the reconstructed images. Like Karras, we calculated PPL based on path endpoints in W and without the central crop. Results are presented in Table 1.

Table 1: Training Results. For each training run, we selected the final training snapshot to evaluate the metrics. A lower FID indicates that the generator produced a distribution of images more similar the training data. A lower PPL indicates the network was better able to generalize onto the training dataset. Best results in each column are indicated in bold.

Network	Dataset	FID	PPL	Training Time (days)
StyleGAN	Simple	3.43	147.25	5d 10h 43m
StyleGAN2*	Simple	3.69	**33.25**	10d 5h 11m
StyleGAN	Augmented	**2.86**	139.34	5d 18h 51m
StyleGAN2*	Augmented	5.70	47.31	11d 23h 28m

* Training results for StyleGAN2 terminated after 21 million image impressions. Results are shown for the last epoch completed.

We presented 80 samples of generated histology and 80 samples of real histology from the training set to a pathologist for evaluation. The pathologist was unable to differentiate between the two groups with 45% prediction accuracy.

The original StyleGAN results include drop-like artifacts resulting from layer signal leakage due to normalization removing channel magnitudes as described in (Karras et al., 2020). We found StyleGAN to generate the same droplike artifacts when trained on prostatic histology and StyleGAN2 to similarly remove these reconstruction artifacts with its improved architecture.

5.2 Style Mixing

To explore the resolution at which various histologic features occur, two randomly-generated histology images were mixed at the inputs to the layers of the generator (Fig. 1). In StyleGAN image synthesis, each input latent code z is converted into a disentangled latent code w by a multi-layered fully-connected network. This w is then inserted into each upsampling convolutional layer twice through style controls. These style controls adjust the mean and standard deviation of each convolutional channel, modifying the signal of specific projected feature maps onto the image.

During style mixing, the w vector for one image is used for most layers, and the w vector for the other image is used for the remaining layers. No truncation adjustment (Karras et al., 2019) was used for these figures. We observe that large scale features (gland, lumen location) are fixed at the course layers of the network (the layers closest to the input). The middle layers control epithelium and stroma textures. The fine layers (those closest to the image) control coloration and nuclear density.

5.3 Capturing Stochastic Variation

In the StyleGAN networks, random noise is broadcast onto each layer to capture stochastic information, such as the exact location of hair or freckles that doesn't change the overall appearance of an image (Karras et al., 2019). Unlike natural images which use a standard composition for the subject, histologic tile samples are truly spatially invariant. Indeed, the precise locations of nuclei, cell boundaries, and glands are modeled through the random channel. Figure 2 shows the effect of varying the input noise while leaving the latent codes intact. It illustrates how the style (inclusion/exclusion, color, thickness, texture) of cells and glands is fixed by the latent code, but the locations are specified by the random broadcast noise.

5.4 Classifying Generated Histology

Given 100 tissue samples, samples were grouped 8 distinct classes. We then averaged all w coordinates each class and projected the mean into an image. Results are shown in Figure 3.

5.5 Generator Interpolation

The network has the ability to create realistic images from latent codes that fall within the latent space. Given two separate image samples, we have shown the impact of style mixing when reconstructing those images given the same latent code. With our work we additionally investigate the impact of defining new latent codes that exist along the path between labeled latent codes (Fig. 4). Although the intermediary samples are independently photorealistic, we find the shortest path in latent space does not capture realistic biochemical transitions in the underlying pathology.

6 DISCUSSION

While histology shares many characteristics in common with natural images (such as containing lines, edges, and RGB color), there are many unique characteristics that differentiate histology generation from natural image generation. Progressive growing or resolution enhancement during training enabled high-resolution image generation that captures histologic structures at multiple scales. By training first on a

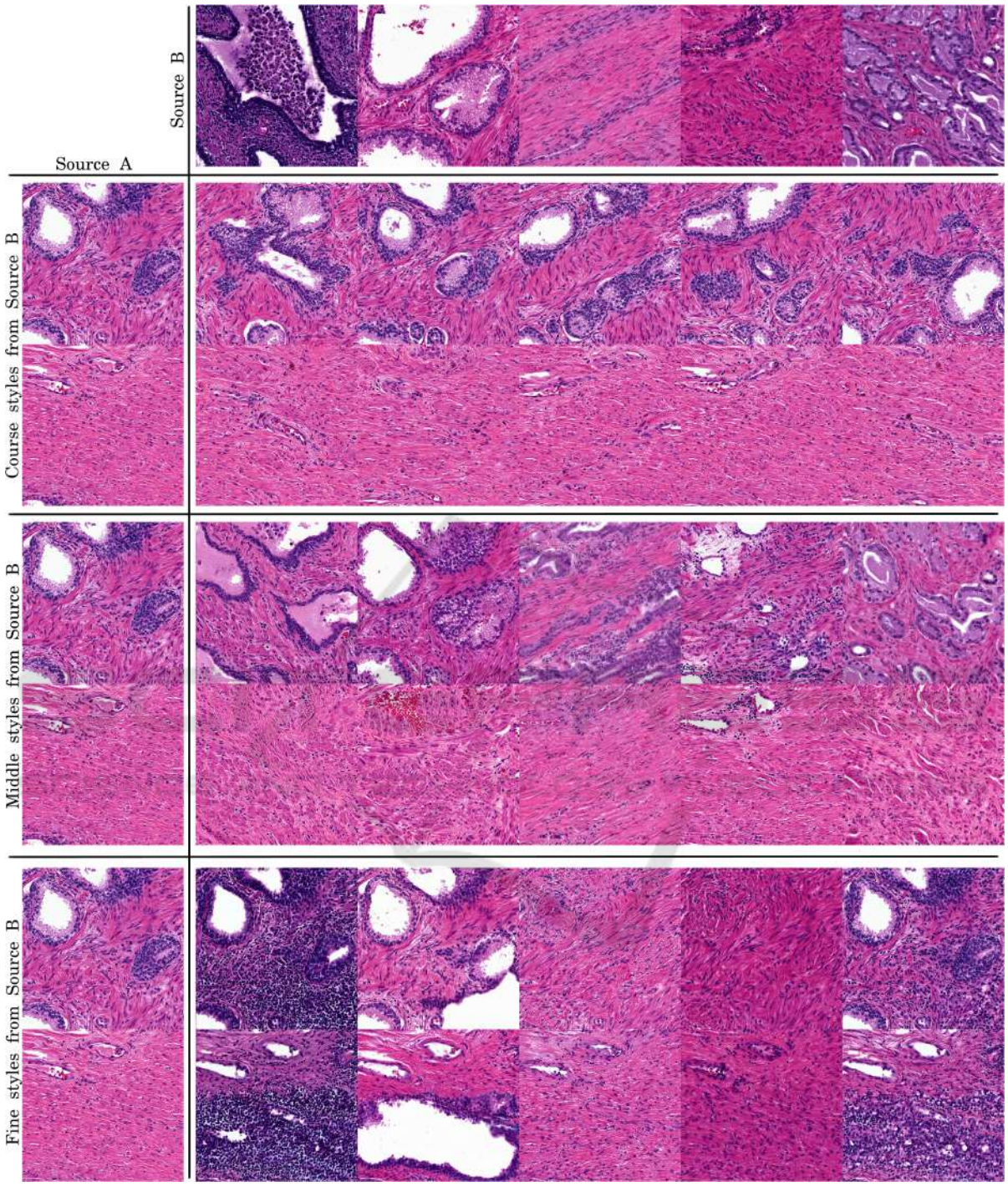

Figure 1: Disentangled latent mixing at generator levels. Using the same approach as the original StyleGAN literature(Karras et al., 2019; Karras et al., 2020), we select two random input latent vectors z, generate pure images, then mix a select set of w vectors from source B into source A at certain layers. In coarse styles, we mix B's w layers into A layers 4^2 to 16^2. In middle styles, B mixed in at 16^2 to 128^2. In fine styles, B mixed into all layers after 128^2. Figure generated with StyleGAN2 on Simple dataset.

course resolution, the network embeds high-level histologic features such as lumen or tissue mass into coarse layer feature maps. Middle layers capture stroma and epithelium textures. Later layers capture low-level fine details like tissue color. Karras et al. hypothesize that lower-resolution data is more sta-

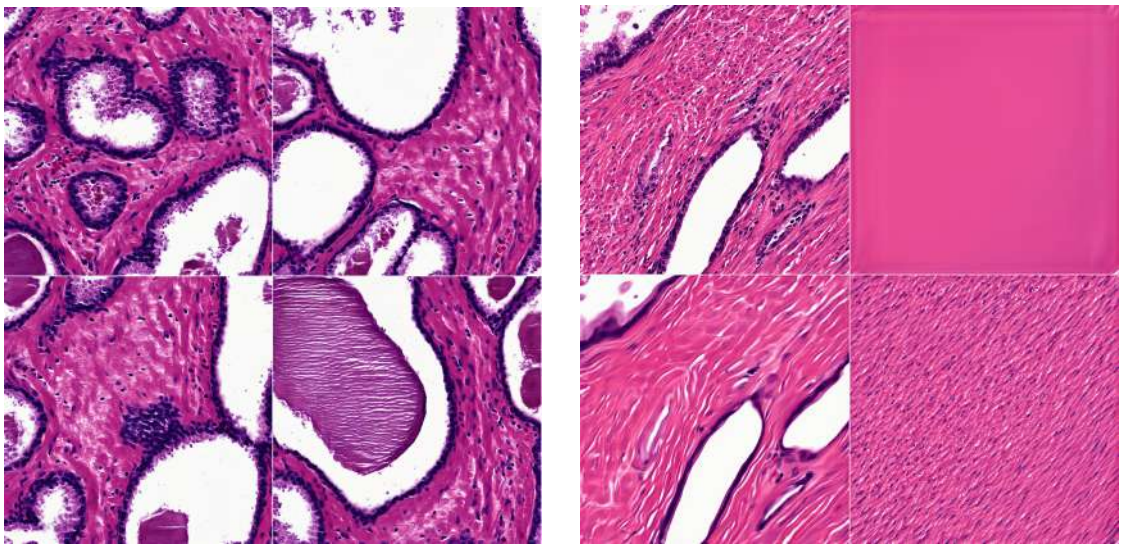

(a) (b)

Figure 2: Impact of random noise on histologic features. (a) Varying input noise. Images are generated from the same latent code but different noise at all layers. Noise impacts multi-scale changes in final image reconstruction, but does not change many of the features important for diagnosis including cell texture and epithelium thickness. (b) Isolating input layers. In the upper left image, all noise input is on. In the upper right image, all noise input is off. In the lower left image, noise is inserted only into the coarse layers. In the lower right image, noise is inserted into only the fine layers. The random input in the course layers control gland placement while those in the fine layers control cell placement.

ble to learn because there are fewer modes, and as learning progresses the modes divide while maintaining the structure shared by the modes (Karras et al., 2018). The course layer feature maps learned early in training provide scaffolding for the later layer feature maps to project more complex fine details.

Although not designed explicitly for spatially invariant cellular medical domains, the StyleGAN is successfully able to isolate stochastic information in the synthesis network noise channels. The noise can be adjusted to dramatically change the appearance of the generated histology without changing the histopathology. A latent code will generate similar histologic morphologies regardless of the random broadcast noise. Additionally, the computer vision improvements in StyleGAN2 with PPL and image artifact reduction carry over in the histology domain.

Conclusion. We have demonstrated that StyleGAN and StyleGAN2 generate realistic prostatic histology at high-resolution (1024^2 images). The GANs capture prostatic structure at multiple scales ranging from gland layout through nuclei density. Image features can be controlled by interpolating between points within the latent space, mixing the inputs to the layers of the generator network, and adjusting the seed for broadcast random noise at different scales.

Future Work. GANs hold much promise for providing interpretation of image data. Central to interpretability is the projection of real clinical images onto the projector's latent space. This would enable pathologists to insert real image specimens into the network for analysis. Extending the StyleGAN2 to learn an image-by-image inverse projection of the generator during training, similar to (Chen et al., 2018) would enable this. A network that produces semantic masks or captions from the generator such as epithelium or stroma segmentation would also enhance the interpretability of the network. Interpolation in latent space could provide insight into disease progression or production of 3D volumes between histology slices. With pathologist collaboration, a more rigorous analysis of the generator network convolutional feature maps in latent clusters may provide insight into the correlation of new Gleason patterns with Gleason grading. Although the default StyleGAN configurations demonstrated success, additional exploration in the length of the transformer network and quality of the dataset could yield improved effectiveness. With additional compute resources and high quality prostatic histology, it is possible the StyleGAN network may show stable image reconstruction at higher 4096^2 resolution.

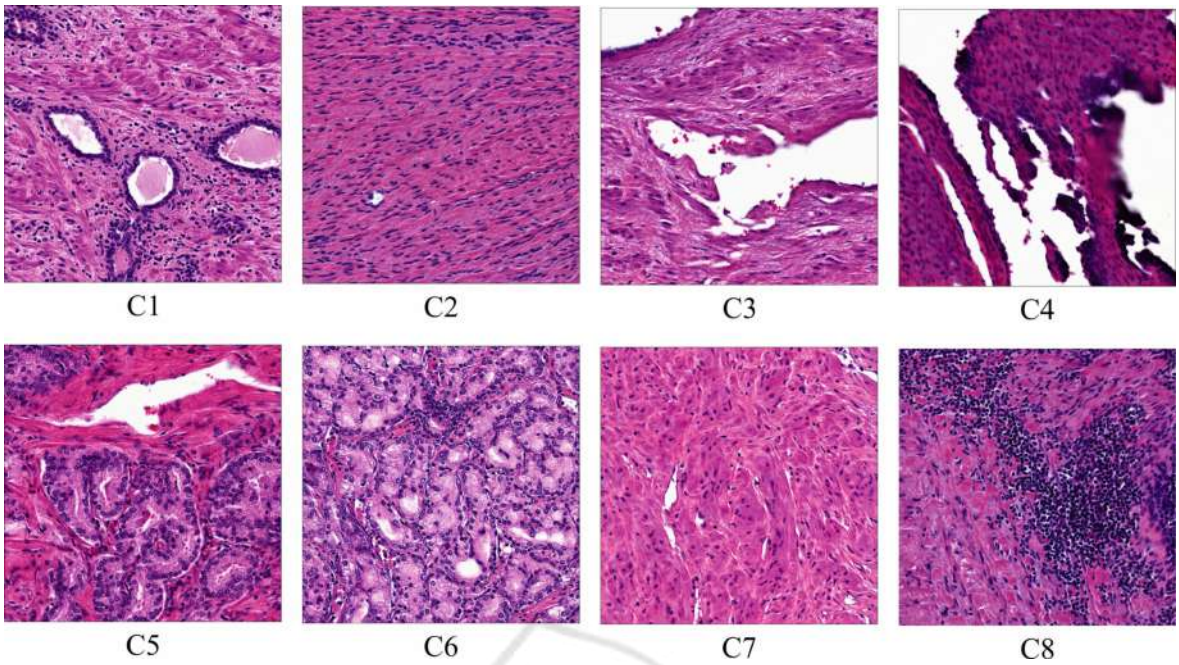

Figure 3: Histologic Morphology Means. Resulting generated histology from mean latent space vectors generated from empirically categorized histologic classes. C2 and C7 mimic stroma, C4 mimics inked prostatic edge, C8 lymphocyte inflammation and C5 and C6 prostatic cancer. StyleGAN2 *Simple* Datset.

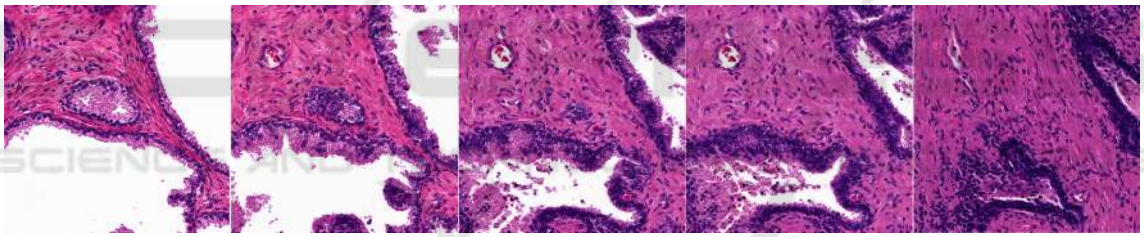

Figure 4: Interpolating between two latent code representations of histologic tiles (Sec. 5.5).

ACKNOWLEDGEMENTS

Funding: The State of Wisconsin Tax Check-off Program for Prostate Cancer Research, NCI/NIH RO1CA218144 (LaViolette), and MSOE Professional Summer Development Funding (Yoder). We would like to thank Allison Lowman for assistance with obtaining the dataset and Samuel Bobholz for insight into data preparation strategy. We would like to thank Dr. John Bukowy for domain expertise and Dr. Sean McGarry for insights into the clinical applications of deep networks.

REFERENCES

Araújo, T., Aresta, G., Castro, E., Rouco, J., Aguiar, P., Eloy, C., Polónia, A., and Campilho, A. (2017). Classification of breast cancer histology images using convolutional neural networks. *PLOS ONE*, 12(6):1–14.

Chen, J., Xie, Y., Wang, K., Wang, Z. H., Lahoti, G., Zhang, C., Vannan, M. A., Wang, B., and Qian, Z. (2018). Generative Invertible Networks (GIN): Pathophysiology-Interpretable Feature Mapping and Virtual Patient Generation. *arXiv:1808.04495*.

Chen, N. and Zhou, Q. (2016). The evolving Gleason grading system. *Chinese Journal of Cancer Research*, 28(1):58–64.

Du, M., Liu, N., and Hu, X. (2019). Techniques for Interpretable Machine Learning. *arXiv:1808.00033 [cs, stat]*.

Goodfellow, I. J., Pouget-Abadie, J., Mirza, M., Xu, B., Warde-Farley, D., Ozair, S., Courville, A., and Bengio, Y. (2014). Generative Adversarial Networks. *arXiv:1406.2661*.

Gutman, D. A., Khalilia, M., Lee, S., Nalisnik, M., Mullen, Z., Beezley, J., Chittajallu, D. R., Manthey, D., and Cooper, L. A. (2017). The digital slide archive: A

software platform for management, integration, and analysis of histology for cancer research. *Cancer Research*, 77(21):e75–e78.

Heusel, M., Ramsauer, H., Unterthiner, T., Nessler, B., and Hochreiter, S. (2017). GANs Trained by a Two Time-Scale Update Rule Converge to a Local Nash Equilibrium. *arXiv:1706.08500*.

Karras, T., Aila, T., Laine, S., and Lehtinen, J. (2018). Progressive Growing of GANs for Improved Quality, Stability, and Variation. *arXiv:1710.10196 [cs, stat]*.

Karras, T., Aittala, M., Hellsten, J., Laine, S., Lehtinen, J., and Aila, T. (2020). Training Generative Adversarial Networks with Limited Data. *arXiv:2006.06676 [cs.CV]*.

Karras, T., Laine, S., and Aila, T. (2019). A style-based generator architecture for generative adversarial networks. In *Proceedings of the Conference on Computer Vision and Pattern Recognition (CVPR)*.

Karras, T., Laine, S., Aittala, M., Hellsten, J., Lehtinen, J., and Aila, T. (2020). Analyzing and improving the image quality of stylegan. In *Proceedings of the Conference on Computer Vision and Pattern Recognition*, pages 8110–8119.

Kazeminia, S., Baur, C., Kuijper, A., van Ginneken, B., Navab, N., Albarqouni, S., and Mukhopadhyay, A. (2018). GANs for Medical Image Analysis. *arXiv:1809.06222*.

Li, W., Li, J., Sarma, K. V., Ho, K. C., Shen, S., Knudsen, B. S., Gertych, A., and Arnold, C. W. (2019). Path R-CNN for Prostate Cancer Diagnosis and Gleason Grading of Histological Images. *IEEE Transactions on Medical Imaging*, 38(4):945–954.

Martinez, K. and Cupitt, J. (2005). VIPS: a highly tuned image processing software architecture. In *IEEE International Conference on Image Processing (31/08/05)*, pages 574–577.

McGarry, S. D., Bukowy, J. D., Iczkowski, K. A., Unteriner, J. G., Duvnjak, P., Lowman, A. K., Jacobsohn, K., Hohenwalter, M., Griffin, M. O., Barrington, A. W., Foss, H. E., Keuter, T., Hurrell, S. L., See, W. A., Nevalainen, M. T., Banerjee, A., and LaViolette, P. S. (2019). Gleason Probability Maps: A Radiomics Tool for Mapping Prostate Cancer Likelihood in MRI Space. *Tomography*, 5(1):127–134.

MICCAI (2020). Kaggle MICCAI 2020 prostate cancer challenge.

Quiros, A. C., Murray-Smith, R., and Yuan, K. (2020). PathologyGAN: Learning deep representations of cancer tissue. *arXiv:1907.02644 [cs, eess, stat]*.

Rawla, P. (2019). Epidemiology of Prostate Cancer. *World Journal of Oncology*, 10(2):63–89.

Skandarani, Y., Painchaud, N., Jodoin, P.-M., and Lalande, A. (2020). On the effectiveness of GAN generated cardiac MRIs for segmentation. *arXiv:2005.09026*.

Xu, Z., Wang, X., Shin, H.-C., Yang, D., Roth, H., Milletari, F., Zhang, L., and Xu, D. (2019). Correlation via synthesis: end-to-end nodule image generation and radiogenomic map learning based on generative adversarial network. *arXiv:1907.03728 [cs, eess]*.

Young, K., Booth, G., Simpson, B., Dutton, R., and Shrapnel, S. (2019). Deep neural network or dermatologist? *arXiv:1908.06612*.

APPENDIX

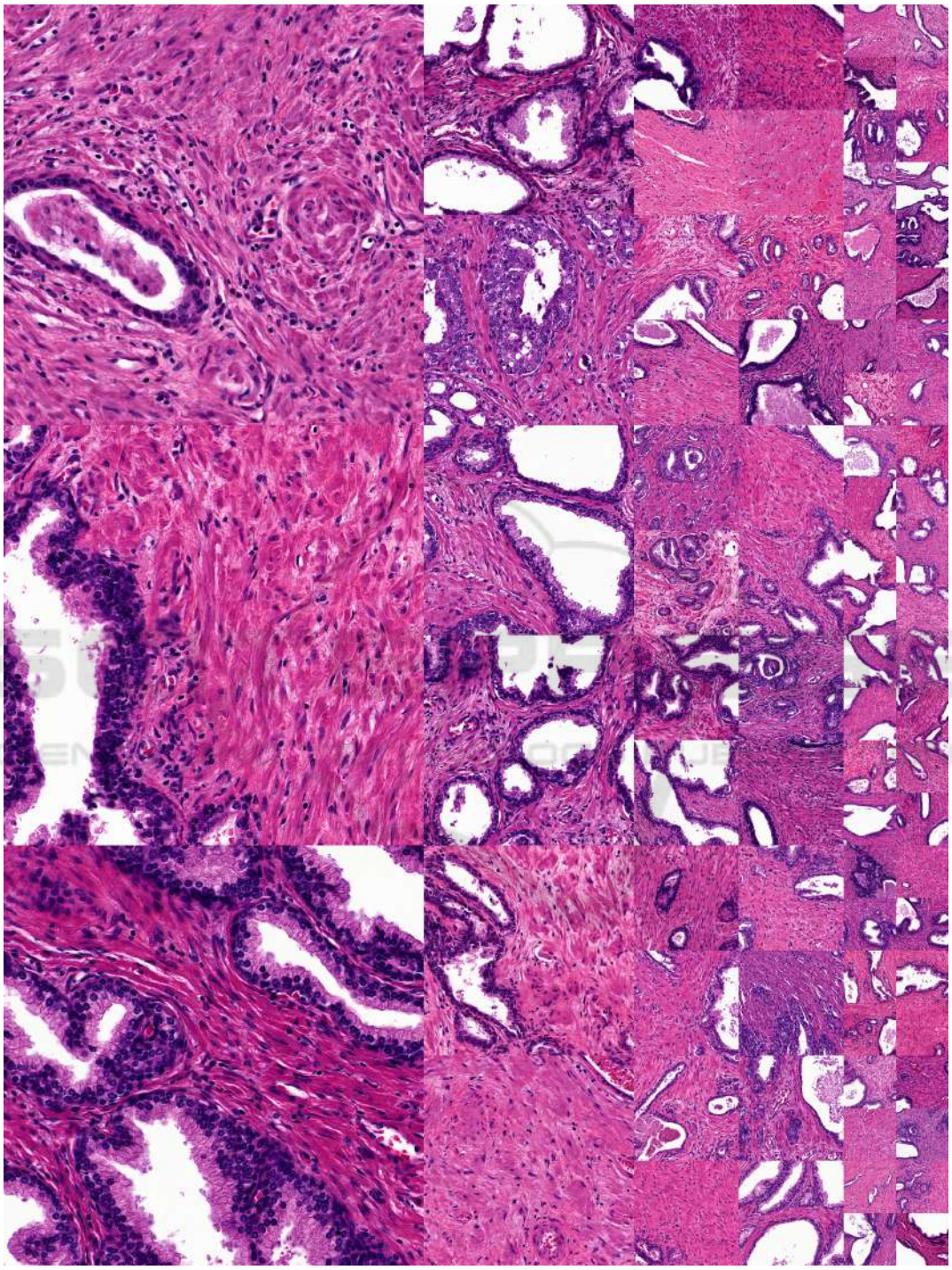

Figure 5: Uncurated random generated histology samples from StyleGAN2 trained on the Simple dataset.

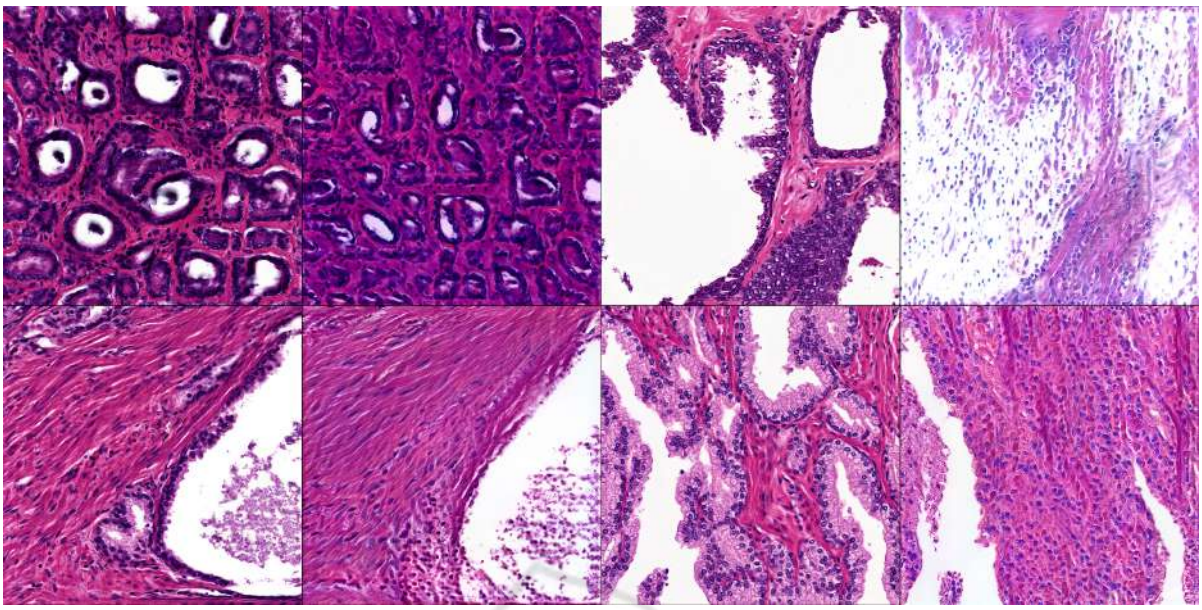

Figure 6: Preliminary experiments with inversion of images. In each pair of images, the image on the left is a generated synthetic image used as an input and the image on the right is the result of the inversion process. To invert images, we used the inversion algorithm in the NVLabs StyleGAN2 package. This adjusting the latent codes through backpropagation to produce an output image as close to the input image as possible. We display this output image as the result of the inversion process. Since the input image is generated by the algorithm, a latent code to generate a perfect match exists, but the inversion process fails to find it. With some tuning, we were able to converge on the correct location of the glands and general color scheme, but the structure of the epithelium tissue is often completely absent. We used our StyleGAN2 network trained on the *Simple* dataset with a truncation scaling factor $\psi = 1.0$ (no scaling).

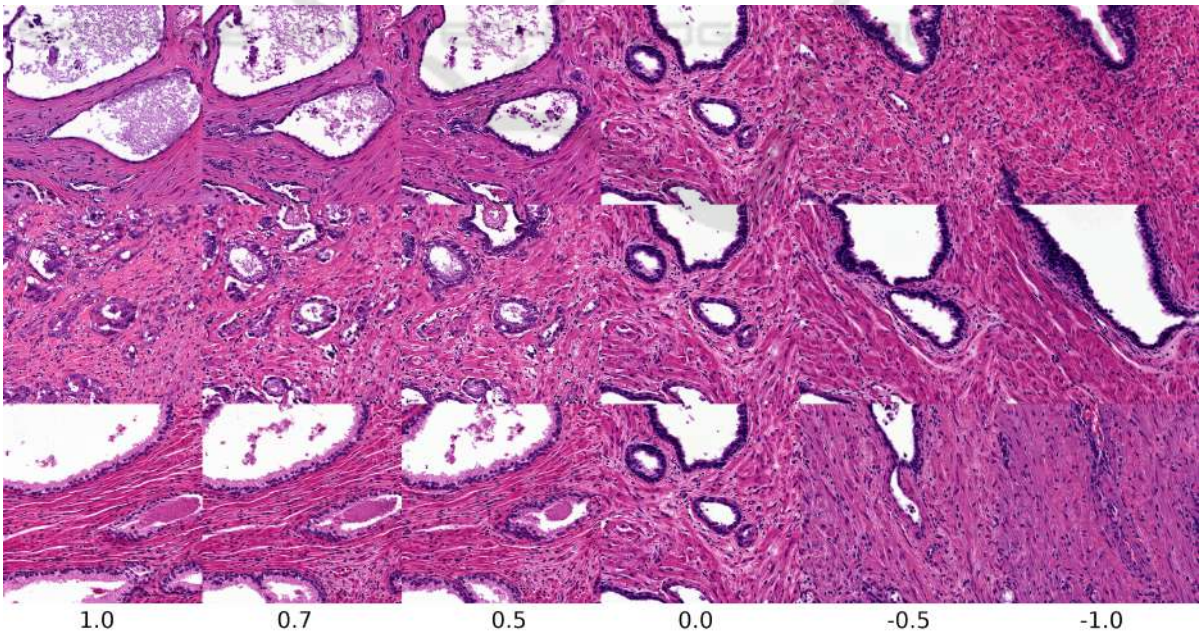

Figure 7: Exploring truncation psi trick on the *Simple* histology dataset with StyleGAN2. As $\psi \rightarrow 0.0$, all histology samples converge to the "mean" histology image in our training dataset. As ψ becomes negative, features are often replaced with their opposites, such as thick vs. thin epithelium and large vs. small or absent glands.